Ultrasonics Sonochemistry 89 (2022) 106162

Contents lists available at ScienceDirect

Ultrasonics Sonochemistry

journal homepage: www.elsevier.com/locate/ultson

Theoretical and experimental investigations on rotary ultrasonic surface micro-machining of brittle materials

Yunze Li [a], Dongzhe Zhang [a], Hui Wang [b], Gaihua Ye [c], Rui He [c], Weilong Cong [a,*]

[a] Department of Industrial, Manufacturing, and Systems Engineering, Texas Tech University, Lubbock, TX 79409, USA
[b] Department of Industrial & Systems Engineering, Texas A&M University, College Station, TX 77843, USA
[c] Department of Electrical & Computer Engineering, Texas Tech University, Lubbock, TX 79409, USA

ARTICLE INFO

Keywords:
Brittle material
Rotary ultrasonic surface micro-machining
Cutting force
Cutting surface quality
Residual stress

ABSTRACT

Many brittle materials, such as single-crystal materials, amorphous materials, and ceramics, are widely used in many industries such as the energy industry, aerospace industry, and biomedical industry. In recent years, there is an increasing demand for high-precision micro-machining of these brittle materials to produce precision functional parts. Traditional ultra-precision micro-machining can lead to workpiece cracking, low machined surface quality, and reduced tool life. To reduce and further solve these problems, a new micro-machining process is needed. As one of the nontraditional machining processes, rotary ultrasonic machining is an effective method to reduce the issues generated by traditional machining processes of brittle materials. Therefore, rotary ultrasonic micro-machining (RUμM) is investigated to conduct the surface micro-machining of brittle materials. Due to the small diameter cutting tool (<500 μm) and high accuracy requirements, the impact of input parameters in the rotary ultrasonic surface micro-machining (RUSμM) process on tool deformation and cutting quality is extremely different from that in rotary ultrasonic surface machining (RUSM) with relatively large diameter cutting tool (~10 mm). Up till now, there is still no investigation on the effects of ultrasonic vibration (UV) and input variables (such as tool rotation speed and depth of cut) on cutting force and machined surface quality in RUSμM of brittle materials. To fill this knowledge gap, rotary ultrasonic surface micro-machining of the silicon wafer (one of the most versatile brittle materials) was conducted in this study. The effects of ultrasonic vibration, tool rotation speed, and depth of cut on tool trajectory, material removal rate (MRR), cutting force, cutting surface quality, and residual stress were investigated. Results show that the ultrasonic vibration could reduce the cutting force, improve the cutting surface quality, and suppress the residual compressive stress, especially under conditions with high tool rotation speed.

1. Introduction

Micro-machining is the machining technology that fabricates high-precision devices or features in the micron size ranges. [1,2]. The tools for the micro-machining process are usually smaller than 500 μm in diameter [3]. Micro-machining has been widely used in the energy industry, aerospace industry, and biomedical industry [4–8]. Brittle materials are widely used in these industries, such as single crystal materials, amorphous materials, and ceramics. For example, micro-features are needed to be machined into optical components (lenses and fibers) for sensor applications. In addition, bone micro-machining applications are commonly used in dentistry and orthopedic surgeries [9].

However, brittle materials (e.g., silicon wafers, sapphire wafers, and SiC wafers) are difficulted to machine due to their low fracture toughness. Microcracking and chipping being commonly generated on the machined surface lead to lower product quality and a higher rejection rate of machined parts [10]. In addition, the traditional micro-machining process also induces residual stress on the material surface, which has negative impacts on the mechanical and optical properties.

In recent years, the non-traditional machining (NTM) processes for silicon wafers have been widely investigated and rapidly developed [11–14]. The commonly used NTM processes are as follows: chemical NTM methods (such as chemical wet etching method and electrochemical machining method) and thermal NTM methods (such as laser-based machining methods). Although the chemical wet etching method

* Corresponding author.
E-mail address: weilong.cong@ttu.edu (W. Cong).

https://doi.org/10.1016/j.ultsonch.2022.106162
Received 30 June 2022; Received in revised form 22 August 2022; Accepted 8 September 2022
Available online 12 September 2022

and electrochemical machining method have the advantages of almost no damage, they still have significant disadvantages of low processing speed, hard to be controlled, and high chemical disposal costs. The thermal NTM methods have the shortcoming of the formation of the heat-affected zone around the laser scanning path, which could reduce the strength of the silicon wafers. In addition, the thermal NTM methods also have disadvantages of hard-to-machine surfaces and complex contours, high specific power consumption, and high initial equipment cost. Therefore, it is necessary to investigate machining methods that have a smoother cutting surface with few microcracking and chipping, lower cost, higher efficiency, and without heat-affected zone.

To reduce or overcome these issues from the traditional micro-machining process and NTM micro-machining process, the mechanical NTM micro-machining processes have been proposed. It is reported that abrasive jet machining (AJM) and abrasive water jet (AWJ) machining have been used in the micro-machining of brittle materials [15–17]. The common limitation associated with both AJM and AWJ is that free abrasive after jetting reduces the accuracy of machined features. In addition, a metal mask or shim needs to be prepared in AJM. The thermal NTM method (such as laser machining) removal of materials by melting/vaporization, has disadvantages of unwanted material oxidation, heat-affected zone, high radiation energy requirement, etc. [18]. Chemical NTM processes such as wet etching, are not feasible for the fabrication of micro-features with a high aspect ratio due to the low material removal rate [19,20]. In recent few decades, a micro ultrasonic machining (μUSM) system has been developed for micro-electromechanical system (MEMS) applications. The shortcoming of μUSM includes free abrasive slurry usage, difficulty to exit the cutting chips, low material removal rates (MRR), etc. It is crucial to investigate an effective and efficient mechanical NTM process. Rotary ultrasonic micro-machining (RUμM) is such a process.

Ultrasonic vibration (abbreviated to “UV” in all Figures), with a frequency higher than 20 kHz, has a positive influence on many manufacturing processes. The frequency of ultrasonic vibration is much higher than the natural frequency of the machine or the manufacturing system. Therefore, different from low-frequency vibration, ultrasonic vibration will not have negative effects on the stability of the processing system [21]. RUμM is a hybrid machining process, in which the material removal consists of traditional grinding and ultrasonic machining [22]. Compared with the traditional machining process, the RUμM process has the advantages of better cutting surface quality with fewer microcracks and chips and lower cutting force and tool wear [23]. At the same time, RUμM also has the advantages of traditional machining. Compared with the chemical wet etching method and electrochemical machining method, the RUμM process has the advantages of higher machining speed, lower cost, and capability of machining complex and small features [24]. Compared with the electrical discharge machining and jet electrolytic drilling method, the advantages of RUμM are also obvious, RUμM can be applied to a wider range of applications, such as drilling, cutting, and grinding. Compared with the laser-based machining process, the RUμM does not cause the heat-affected zone, which could increase the strength of the silicon wafers and improve the assembly performance [25]. Owing to these advantages, RUμM is a potential method for machining silicon wafers.

There are many reported investigations on rotary ultrasonic machining (RUM) of brittle materials with large-scaled cutting tools (cutting tool diameter ~10 mm). Results show that with ultrasonic vibration, the cutting force will be reduced and the quality of the end surface will be improved [23]. In addition, the effects of tool rotation speed, feed rate, ultrasonic power, and coolant pressure on the material removal rate and surface quality of RUM have been investigated [26,27]. It has been reported that among them, tool rotation speed was the input parameter that has a great influence [28]. Compared with the RUM process, the cutting tool size in the RUμM process is much smaller (<500 μm diameter). Due to the extremely small cutting tool size, under the same level of tool rotation speed, the line speed of abrasive grains is much lower than that in the RUM process. Thus, the quality of the end surface is more sensitive to the tool rotation speed. In addition, due to the small cutting tool diameter, the vertical cutting force may cause deformation of the tool and thus reduce the machining quality. Due to these reasons, the effects of ultrasonic vibration and input parameters on cutting force and machining quality still need to be investigated. However, the reports on the RUμM process are still limited [29]. The hole drilling using RUμM developed from micro-ultrasonic machining (μUSM) with workpiece ultrasonic vibration has been reported [30]. A statistic model was built for wear in multi-abrasive tools. A comparison between the micro-grinding and RUμM was conducted and showed that the RUμM reduced the cutting force and suppressed the phenomenon of edge chipping [31]. As far as authors know, there is no investigation on the rotary ultrasonic surface micro-machining (RUSμM) of brittle materials by using abrasive cutting tools. The effects of ultrasonic vibration and input parameters on the cutting surface quality, cutting force, and MRR in RUSμM process urgently need to be investigated.

Silicon and silicon-based wafers, as a kind of brittle material, have been widely used in photovoltaic, semiconductor, medical, aerospace, and optical industries [4,14]. For example, to reduce pollution and the greenhouse effect through the combustion process silicon wafer is commonly used in solar cell techniques to convert solar energy into electricity [5]. Currently, only about one-sixth of the sunlight entering a typical solar panel can be converted into electricity. Improving the efficiency of solar cells and reducing the manufacturing cost of solar panels become the main challenges associated with solar panels [13]. In order to create a low-reflectivity texture on the surface of silicon solar cells and improve the efficiency of silicon-based solar cells, the fabrication of a low-reflectivity texture on the surface of the silicon wafer was needed. This requires high-precision surface micro-machining technologies.

To fill this knowledge, in this study, the silicon wafers were surface machined by the RUSμM process with different tool rotation speeds and depths of cut with and without ultrasonic vibration. The single diamond scratching tests were conducted to investigate the effects of ultrasonic vibration and single abrasive indentation depth on the vertical scratching force and scratch-induced features. The trajectory lengths of tool abrasive grain and the vertical cutting forced under different input parameters with and without ultrasonic vibration were modeled. The theoretical trajectory lengths of tool abrasive grain, single abrasive indentation depth, and vertical cutting forces were utilized to further investigate and explain the effects of ultrasonic vibration and input variables on the MRR, vertical cutting force, edge chipping, cutting surface quality, and residual stress in the RUSμM process.

2. Workpiece materials, experimental setup, and measurement procedures

2.1. Experimental setup

As shown in Fig. 1, a Sonic-Mill (Series 10) rotary ultrasonic machine (Albuquerque, NM, USA) was used to conduct the RUSμM experiments. The RUSμM system mainly consists of four systems: an ultrasonic tool rotation system, a coolant system, and a data acquisition and horizontal feeding system. The ultrasonic tool rotation system included a controller, an ultrasonic generator, and an electric motor. The controller was used to control the ultrasonic power and other input variables. The ultrasonic generator was used to provide the ultrasonic vibration, which was then transmitted to the cutting tool. The electric motor was used to provide the tool rotation speed. The coolant system consisted of a coolant tank, a pump, tubes, etc., which were used to reduce the temperature of the electric motor. The data acquisition system was used to obtain the vertical cutting force during the RUSμM process, which would be discussed in the measurement section. The horizontal feeding system included a linear stage, a motor controller, and software. The linear stage provided a uniform horizontal feed to realize the RUSμM process.

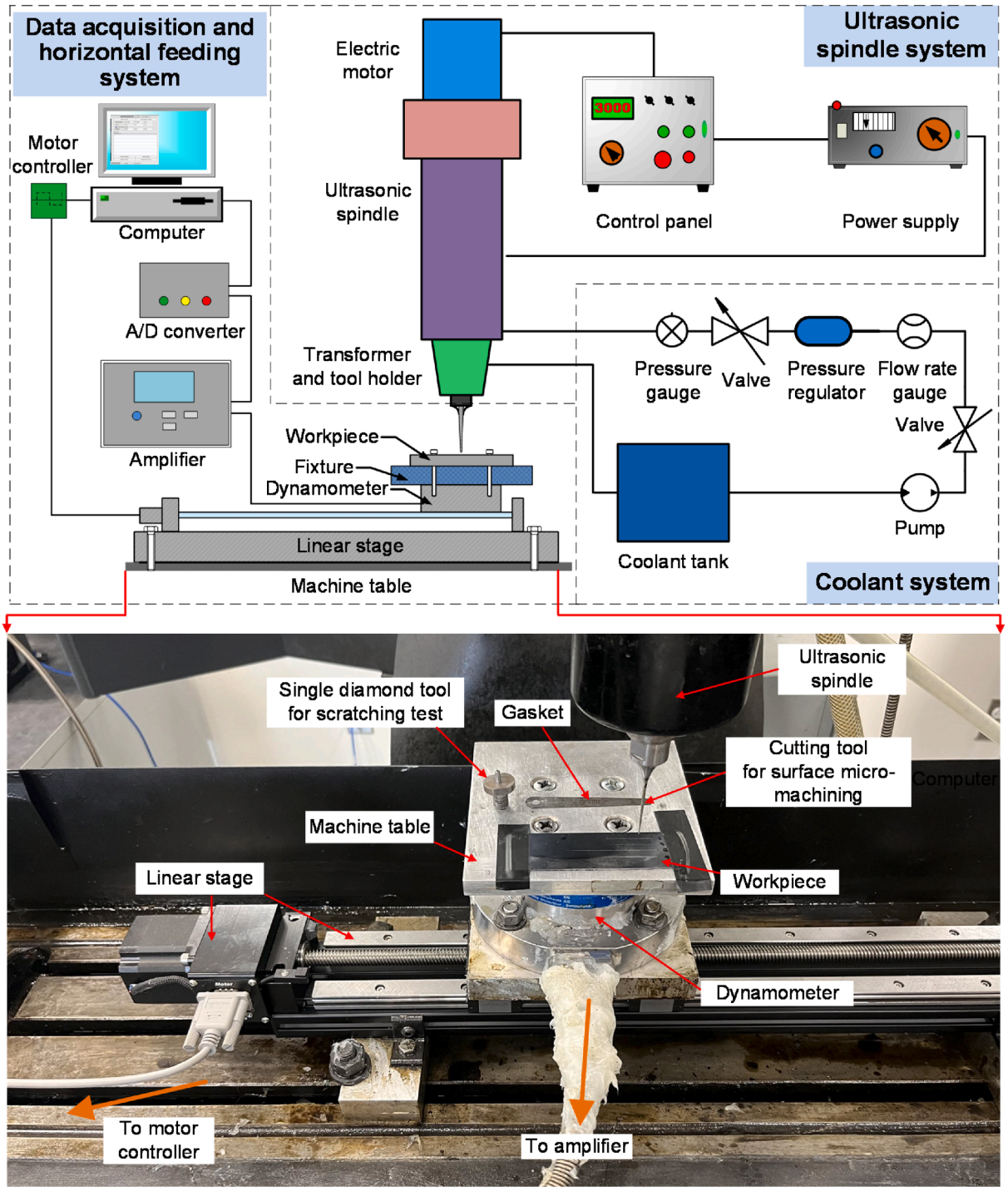

Fig. 1. The illustration and photograph of the experimental setup for the rotary ultrasonic micro-machining (RUSμM) process.

In this investigation, the workpiece was the single side polished circular silicon wafer in (100) crystal orientation with a thickness of 1000 μm (UniversityWafer, Inc., USA). The ultrasonic vibration has a frequency of 20 kHz and an amplitude of 4 μm, respectively. The feeding motion was generated by the combination of a linear stage, an NSC-A1 motion controller, and QuickMotion software (Dslide, Newmark, USA). A diamond burrs bit (Uxcell corp., China) was used to conduct the surface micro-machining process. It could be seen that the diamond abrasives with a diameter of about 75 μm were uniformly fixed on the surface of the cutting tool. A single diamond dresser (Praztech, Switzerland) with a 90° of include angle was used to conduct the single diamond scratching tests. The detailed variables of the cutting tool and single diamond tool were shown in Fig. 2.

For the surface micro-machining process, the surface of the workpiece was kept horizontal to produce the surface micro-machined regions with a consistent depth of cut. The silicon wafer was fixed to the machine table using strong adhesive tape to ensure a tight connection between the silicon wafer and the machine table. Before the experiment, the digital indicator (ID-S112, Mitutoyo Corp., Japan) was used to measure the height difference between the two ends of the silicon wafer and ensure that the height difference was less than 2 μm. The cutting tool was set in the middle of the silicon wafer by changing the position of

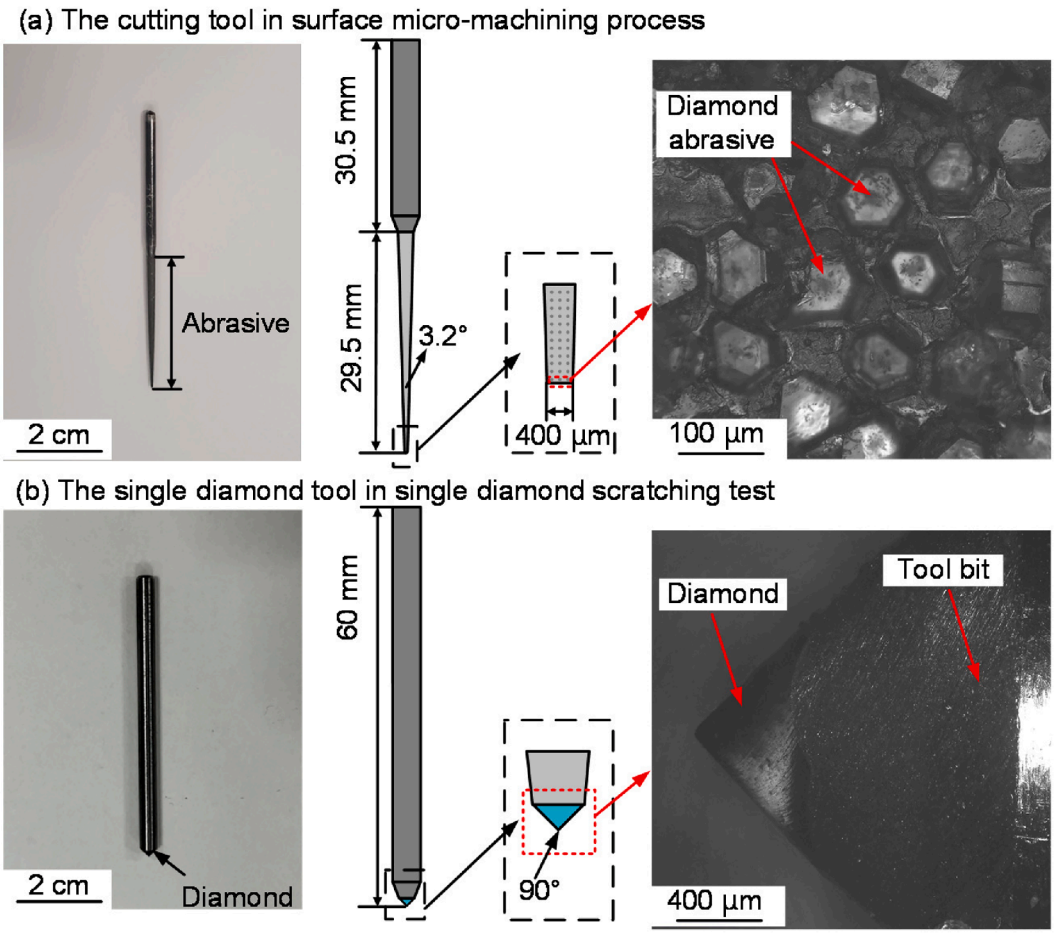

Fig. 2. The illustrations and OM images of (a) the cutting tool used in surface micro-machining process and (b) the single diamond tool used in single diamond scratching test.

the machine table. Then, the machine table was moved up until the cutting tool lightly touched the surface of the silicon wafer. The contact between the cutting tool and the silicon wafer was detected by the data acquisition system which was capable of detecting a force of less than 0.01 N. The upward movement of the machine table was stopped when the data acquisition system indicated a force of around 0.1 N. After that, the cutting tool was offset to the outside of the silicon wafer. The machine table was moved up the distance according to the depth of cut of the experimental design. The rotation of the cutting tool was set to the desired speed and ultrasonic vibration was selected to be turned on or off depending on the experimental parameters. After the rotation speed was stable, the transverse surface micro-machining process was performed. During the experiment, the linear stage drove the machine table, silicon wafer, and dynamometer in the horizontal direction at a constant speed. With the completion of this process, the surface micro-machining regions with a consistent depth of cut were produced. Table 1 lists the detailed machining variables of each group. The selection of these values was optimized and selected according to the previous investigations and preliminary tests. For each combination of processing variables, the experiment was repeated five times to minimize the error.

For single diamond scratching tests, the right end of the silicon wafer was raised using a 20 μm thick gasket and then the silicon wafer was fixed on the machine table using strong adhesive tape. The digital indicator (ID-S112, Mitutoyo Corp., Japan) was used to measure the height difference between the two ends of the silicon wafer and ensure that the height difference was 20 ± 2 μm. The cutting tool was set on the left end of the silicon wafer by changing the position of the machine table. The setup of the contact between the single diamond tool and the silicon wafer was the same as that in the surface micro-machining process. After that, the single diamond tool was offset to the position of 2 mm outside the left edge of the silicon wafer and kept the height unchanged. The single diamond tool was stationary rather than rotating. During the experiment, the linear stage drove the machine table, silicon

Table 1a
Experimental conditions of the surface micro-machining process.

Input fabrication variables	Unit	Values
Feed rate, f_r	mm/s	0.1
Horizontal ultrasonic amplitude, A	μm	4
Ultrasonic power	%	60

Table 1b
Experimental design of the investigation on effects of ultrasonic vibration, tool rotation speed, and depth of cut.

Exp. No.	Ultrasonic vibration	Tool rotation speed (rpm)	Depth of cut (mm)
1	Without	2500	0.2
2	Without	3000	0.2
3	Without	3500	0.2
4	With	2500	0.2
5	With	3000	0.2
6	With	3500	0.2
7	Without	3000	0.1
8(2)	Without	3000	0.2
9	Without	3000	0.3
10	With	3000	0.1
11(5)	With	3000	0.2
12	With	3000	0.3

wafer, and dynamometer in the horizontal direction at a constant speed of 300 mm/s. With the completion of this process, the single diamond scratch-induced features with gradually increasing depth of cut were produced. The experiment was repeated five times. After, the ultrasonic vibration with 60 % power and 4 μm amplitude was turned on and the single diamond scratching test with ultrasonic vibration was conducted. The experiment with ultrasonic vibration was also repeated five times.

2.2. Measurement procedures

The vertical cutting force was collected by the data acquisition system. The data acquisition system consists of a Kistler Type 9272 dynamometer, a Kistler Type 5070 charge amplifier, a Kistler Type 5697A A/D converter, and the DynoWare software (Winterthur, Switzerland). The dynamometer was fixed under the linear stage, which was used to collect the analog signals of the cutting force. The charge amplifier was used to amplify these analog signals. The converter was used to transfer the analog signals into digital signals. The DynoWare software was used to collect and save the cutting force. The typical cutting-force curve during the surface machining process is shown in Fig. 3. Section (1) in Fig. 3 shows the cutting start-time range, which begins at the tool starts to contact the silicon wafers and ends when the tool totally feeds into the silicon wafers. Section (2) in Fig. 3 shows the range when the tool already feeds into the silicon wafers. The averaged cutting force in Section (2) of Fig. 3 was used in this study. An optical microscope (OM) (DSX-510, OLYMPUS, Tokyo, Japan) was used to observe and measure the machined surfaces. The software of this OM (DSX110/510/510i Ver.3.1.3 Version Up Program, OLYMPUS, Tokyo, Japan) was used to process the observed images into 3D-contour images, which could provide more detailed information about the depth and morphologies of the machined surface. A scanning electron microscopy (SEM) (Phenom, Nanoscience, USA) was used to obtain the morphologies of the bottom of the surface micro-machined regions. A Raman spectrometer (HORIBA Jobin Yvon, USA) was used to obtain the Raman spectrum of the regions away from the machined surface and the surface micro-machined regions under different input parameters. In the Raman spectrum tests, five random regions of each sample were measured.

3. Kinematic motion analysis

3.1. Analysis of abrasive grains' trajectory length

3.1.1. Abrasive grains' trajectory length without ultrasonic vibration

In this study, the cutting tool was in a tapered shape. Therefore, the tool radius was related to the depth of cut (*DOC*), which will lead to differences in trajectory length, indentation depth, and cutting force in different regions of the cutting tool. In order to simplify the calculation process, in this study, we analyze the abrasive grains which were located at half of the depth of cut. The tool radius R could be calculated by Eq. (1):

$$R = \frac{2DOCtan(3.2^\circ) + R_B}{2} \tag{1}$$

where, DOC is the depth of cut, mm; R_B is the bottom diameter of the cutting tool, mm.

Surface micro-machining of the silicon wafer with vertical ultrasonic vibration is shown in Fig. 4(a). The tool-abrasive-grain motions were related to the ultrasonic vibration, tool rotation speed, and feedrate. The trajectories of a single abrasive grain without ultrasonic vibration were also shown in Fig. 4(a). The kinematic tool-abrasive-grain trajectory without ultrasonic vibration can be represented as Eq. (2):

$$\begin{cases} x = Rcos\left(\dfrac{\pi St}{30}\right) + f_r t \\ y = Rsin\left(\dfrac{\pi St}{30}\right) \\ z = 0 \end{cases} \tag{2}$$

where, R is tool radius, mm; S is rotation speed of the tool, rpm; f_r is the feed rate, mm/s; t is machining time, s.

The abrasive grain's real-time velocity can be represented as Eq. (3):

$$\begin{cases} v_x = -\dfrac{\pi SR}{30} sin\left(\dfrac{\pi St}{30}\right) + f_r \\ v_y = \dfrac{\pi SR}{30} cos\left(\dfrac{\pi St}{30}\right) \\ v_z = 0 \end{cases} \tag{3}$$

It should be noted that in the case without ultrasonic vibration, there is no one ultrasonic circle time. In order to investigate the abrasive grain's velocity in a simpler way, in this chapter, the time length used for the kinematic motion analysis under the condition without and with ultrasonic vibration was both one ultrasonic cycle. The trajectory length of tool abrasive grain without ultrasonic vibration ($L_{W/O\text{-}UV}$) can be represented as Eq. (4):

$$L_{\mathrm{W/O-UV}} = \int_0^T \sqrt{v_x^2 + v_y^2 + v_z^2}\,dt = \int_0^T \sqrt{\left(\frac{\pi SR}{30}\right)^2 + f_r^2 - f_r \frac{\pi SR}{15} sin\left(\frac{\pi St}{30}\right)}\,dt \tag{4}$$

3.1.2. Abrasive grains' trajectory length with ultrasonic vibration

The trajectories of single abrasive grain with ultrasonic vibration were shown in Fig. 4(a). The kinematic tool-abrasive-grain trajectory with ultrasonic vibration can be represented as Eq. (5):

$$\begin{cases} x = Rcos\left(\dfrac{\pi St}{30}\right) + f_r t \\ y = Rsin\left(\dfrac{\pi St}{30}\right) \\ z = Asin(2\pi ft) \end{cases} \tag{5}$$

where, R is tool radius, mm; A is the ultrasonic amplitude, mm; S is tool rotation speed, rpm; f is the ultrasonic frequency, Hz; f_r is workpiece feed rate, mm/s; t is machining time, s. In this study, the cutting tool was in a tapered shape.

The abrasive grain's real-time velocity can be represented as Eq. (6):

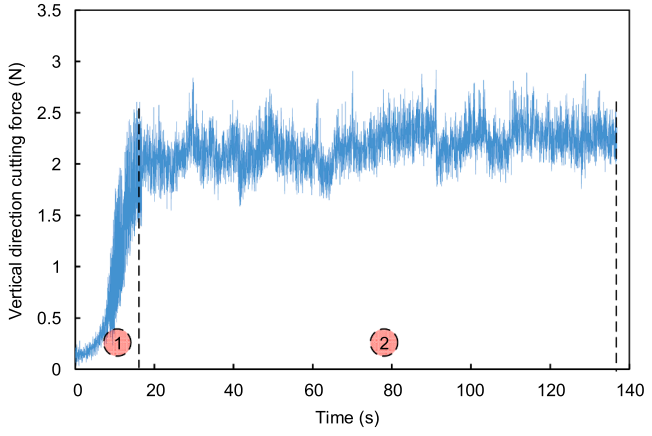

Fig. 3. The typical cutting force curve.

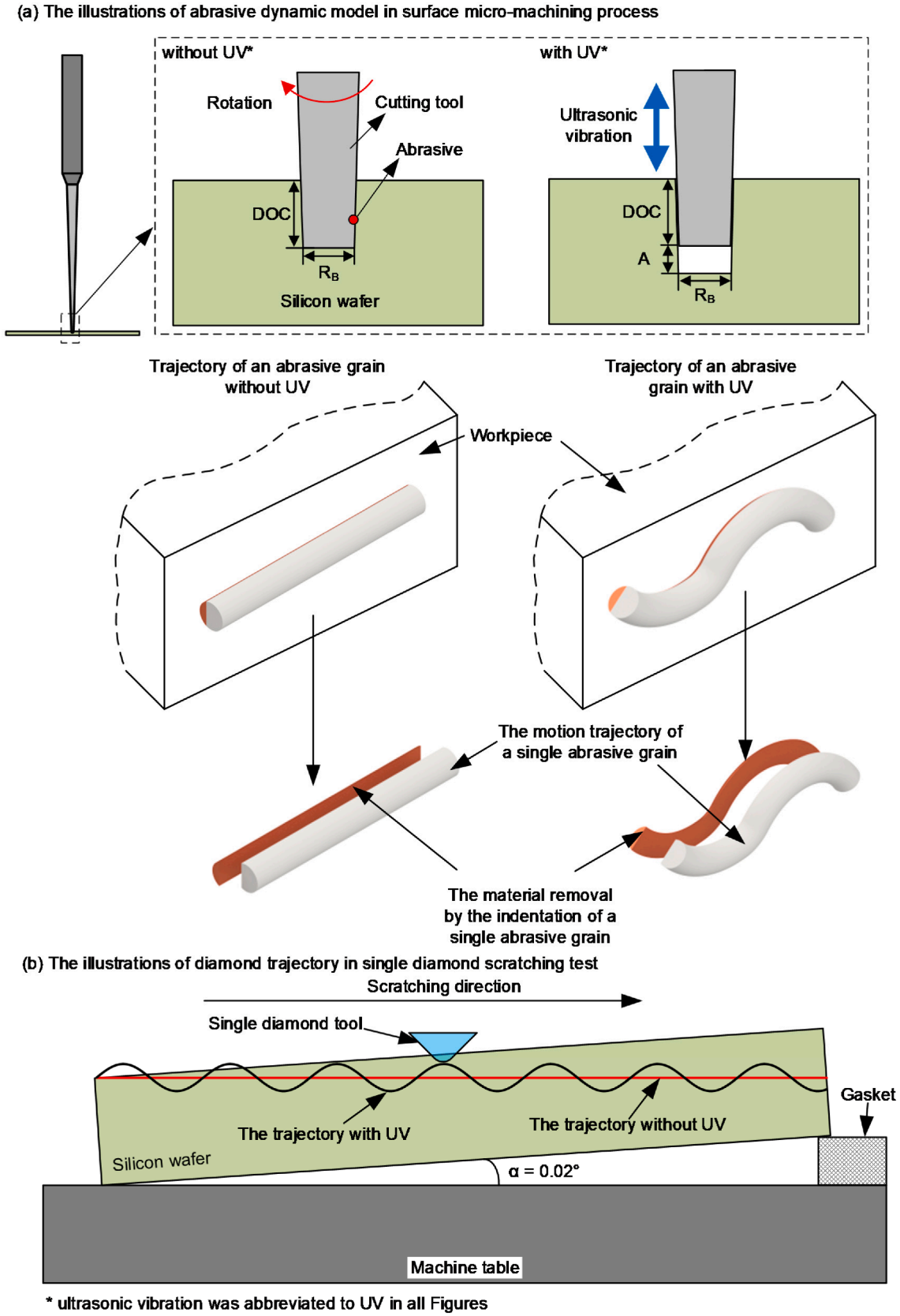

Fig. 4. The illustrations of (a) abrasive dynamic model in surface micro-machining process and (b) diamond trajectory in single scratching test.

$$\begin{cases} v_x = -\dfrac{\pi SR}{30} sin\left(\dfrac{\pi St}{30}\right) + f_r \\ v_y = \dfrac{\pi SR}{30} cos\left(\dfrac{\pi St}{30}\right) \\ v_z = 2\pi fAcos(2\pi ft) \end{cases} \tag{6}$$

The trajectory length of tool abrasive grain with ultrasonic vibration (L_{UV}) can be represented as Eq. (7):

$$L_{UV} = \int_0^T \sqrt{v_x^2 + v_y^2 + v_z^2} dt = \int_0^T \sqrt{\left(\frac{\pi SR}{30}\right)^2 + f_r^2 - f_r \frac{\pi SR}{15} sin\left(\frac{\pi St}{30}\right) + (2\pi fAcos(2\pi ft))^2} dt \tag{7}$$

3.2. Analysis of verticle cutting force

3.2.1. Vertical cutting force without ultrasonic vibration

Under the condition without ultrasonic vibration, the cutting force for each abrasive grain (F_1) can be represented by Eq. (8) [32,33]:

$$F_1 = \frac{8^{1/2} E d^{1/2} \delta^{3/2}}{3(1-\nu^2)} \tag{8}$$

where, E is the elastic modulus of the silicon wafer, ν is the Poisson's ratio of the silicon wafer, and δ is the indentation depth for each abrasive grain, mm.

The trajectory of each abrasive grain without UV were shown in Fig. 4(a). In the surface micro-machining process without ultrasonic vibration, the material removal volume of each abrasive grain (V_1) can be calculated by Eq. (9):

$$V_1 = \frac{1}{2} K_V \pi \left(\frac{F_1}{K_c}\right) (d\cdot\delta - \delta^2) L_{W/O-UV} \tag{9}$$

where, K_V is a constant parameter; KC is the fracture toughness, MPa; δ is the indentation depth for each abrasive grain, mm; d is the abrasive grain's diameter, mm; F_1 is the force for each abrasive grain, N; $L_{W/O\text{-}UV}$ is the trajectory length of tool abrasive grain without ultrasonic vibration.

Summing the V_1 of all abrasive particles could obtain the theoretical MRR, which can be calculated by Eq. (10):

$$MRR = n_s \cdot V_1 \tag{10}$$

where, n_s is the number of active abrasive grains on the cutting tool side.

Multiplying the feedrate and cross-section area of the cutting tool also could obtain the MRR. The MRR can be expressed as Eq. (11):

$$MRR = f_r \cdot DOC \cdot (DOC tan(3.2^\circ) + R_B) \tag{11}$$

where, DOC is the depth of cut set in the experimental design, mm; R_B is the bottom diameter of the cutting tool, mm; R is the tool diameter in the location of the silicon wafer surface.

By combining Eq. (10) and Eq. (11), Eq. (12) with one unknown of δ can be obtained. By solving Eq. (12), the indentation depth for each abrasive grain (δ) can be calculated.

$$\frac{1}{2} n_s K_V \pi \left(\frac{\frac{8^{1/2} E d^{1/2} \delta^{3/2}}{3(1-\nu^2)}}{K_c}\right) (d\cdot\delta - \delta^2) L_{W/O-UV} = f_r \cdot DOC \cdot (DOC tan(3.2^\circ) + R_B) \tag{12}$$

Finally, the axial cutting force ($F_{W/O\text{-}UV}$) under the condition without ultrasonic vibration can be calculated by Eq. (13):

$$F_{W/O-UV} = n_b \cdot F_1 + n_s \cdot F_1 \cdot sin(3.2^\circ) = \frac{8^{1/2} n E d^{1/2} \delta^{3/2}}{3(1-\nu^2)} \cdot (n_b + n_s sin(3.2^\circ)) \tag{13}$$

where, n_b is the number of active abrasive grains on the cutting tool bottom.

3.2.2. Vertical cutting force with ultrasonic vibration

Under the condition with ultrasonic vibration, the force for each abrasive grain (F_1) also can be calculated by Eq. (10). Fig. 4(a) shows the trajectory of each abrasive grain with UV. Similar to the surface micro-machining process without ultrasonic vibration, the material removal volume of each abrasive grain (V_1) with ultrasonic vibration in one ultrasonic cycle can be calculated by Eq. (14):

$$V_1 = \frac{1}{2} K_V \pi \left(\frac{F_1}{K_c}\right) (d\cdot\delta - \delta^2) L_{UV} \tag{14}$$

where, K_V is a constant parameter; KC is the fracture toughness, MPa; δ is the indentation depth for each abrasive grain, mm; d is the abrasive grain's diameter, mm; F_1 is the force for each abrasive grain, N; L_{UV} is the trajectory length of tool abrasive grain with ultrasonic vibration.

Different from the surface micro-machining process without ultrasonic vibration, with the addition of ultrasonic vibration, the MRR should be calculated by Eq. (15):

$$MRR = n \cdot f \cdot V_1 \tag{15}$$

where, n is the number of active abrasive grains.

As shown in Fig. 4(a), in the surface micro-machining with vertical ultrasonic vibration, the actual depth of cut is increased to $DOC + A$. Therefore, by multiplying the feedrate and cross-section area, the MRR should be calculated by Eq. (16):

$$MRR = f_r \cdot ((DOC + A) tan(3.2^\circ) + R_B) \cdot (DOC + A) \tag{16}$$

where, DOC is the depth of cut set in the experimental design, mm; R_B is the tool bottom diameter, mm; R is the tool diameter in the location of the silicon wafer surface.

Similarly, by combining Eq. (15) and Eq. (16), Eq. (17) with one unknown of δ can be obtained, which can be used to calculate the indentation depth of each abrasive grain penetrating into the workpiece (δ) with ultrasonic vibration.

$$\frac{1}{2} n_s f K_V \pi \left(\frac{\frac{8^{1/2} E d^{1/2} \delta^{3/2}}{3(1-\nu^2)}}{K_c}\right) (d\cdot\delta - \delta^2) L_{W/O-UV} = f_r \cdot ((DOC + A) tan(3.2^\circ) + R_B) \cdot (DOC + A) \tag{17}$$

Note that the indentation depth of the Z-direction cannot be obtained directly by this model. We assume that the indentation depth in the X-direction was equal to the indentation depth in the Z-direction, in order to calculate the vertical cutting force. Under the condition with ultrasonic vibration, the axial cutting force (F_{UV}) can be expressed by Eq. (18):

$$\begin{aligned} F_{UV} &= n_b \cdot f \cdot \Delta t \cdot F_1 + n_s \cdot \sin(3.2^\circ) \cdot f \cdot \Delta t \cdot F_1 \\ &= \left[\frac{1}{2} - \frac{1}{\pi} asc\sin\left(1 - \frac{\delta}{A}\right)\right] \frac{8^{1/2} n E d^{1/2} \delta^{3/2}}{3(1-\nu^2)} (n_b + n_s \sin(3.2^\circ)) \end{aligned} \tag{18}$$

4. Results and discussion

4.1. Analysis of single diamond scratching

In order to better understand and analyze the effects of ultrasonic vibration and indentation depth on vertical cutting direction cutting

force, surface micro-machining induced features, and the material removal mechanisms, the single diamond scratch experiment was conducted as shown in Fig. 4(b). By simplifying the complex multi-abrasive surface micro-machining process to a single-abrasive scratching on the material surface, this method made it easier to obtain the scratching forces and scratching morphologies caused by a single abrasive in surface micro-machining and to further analyze the material removal mechanisms [34].

Fig. 5 shows the effects of ultrasonic vibration on the vertical scratching forces and the SEM images of scratching morphologies. As shown in Fig. 5(a), for both conditions with and without ultrasonic vibration, the vertical scratching force increased as the indentation depth increased. The experimentally obtained curves of the vertical scratching force versus indentation depth can be in good agreement with the curves provided by Eq. (8) in the theoretical model. For the same indentation depth, the vertical scratching force under the condition with ultrasonic vibration was always less than that under the condition without ultrasonic vibration. Such a phenomenon indicated that the intermittent contact mode between cutting tool and substrate caused by ultrasonic vibration could reduce the vertical scratching force [35,36]. In addition, the vertical scratching force could be used to determine the material removal mechanisms: small variations in the vertical scratching force implied plastic deformation, while large variations in the vertical scratching force implied the occurrence of brittle fracture [37]. For both conditions with and without ultrasonic vibration, the brittle fracture occurred at an indentation depth of around 1.5 μm.

Fig. 5(b) shows the effects of ultrasonic vibration on the scratch-induced features under the scratching depths of 1, 2, and 3 μm. It could be seen that when the scratching depth was 1 μm, the scratch-induced features without ultrasonic vibration showed smooth surfaces with flat grooves, indicating complete plastic deformation. With the assistance of ultrasonic vibration, the scratch-induced features showed intermittent craters, indicating the occurrence of discontinuous contacts between the cutting tool and substrates. When the scratching depth increased to 2 μm, the microcracks and high brittle portions occurred in the scratch-induced features without ultrasonic vibration, indicating the occurrence of brittle material removal. As a comparison, ultrasonic vibration could significantly inhibit microcracks and high brittle portions [38]. In addition, ultrasonic vibration would cause the scratch-induced surfaces to be more uneven and in wave shapes. When the scratching depth further increased to 3 μm, more microcracks and high brittle portions occurred in the scratch-induced features. The morphologies of the scratch-induced features indicated that with the increase of scratching depth, the material removal mode transferred from plastic

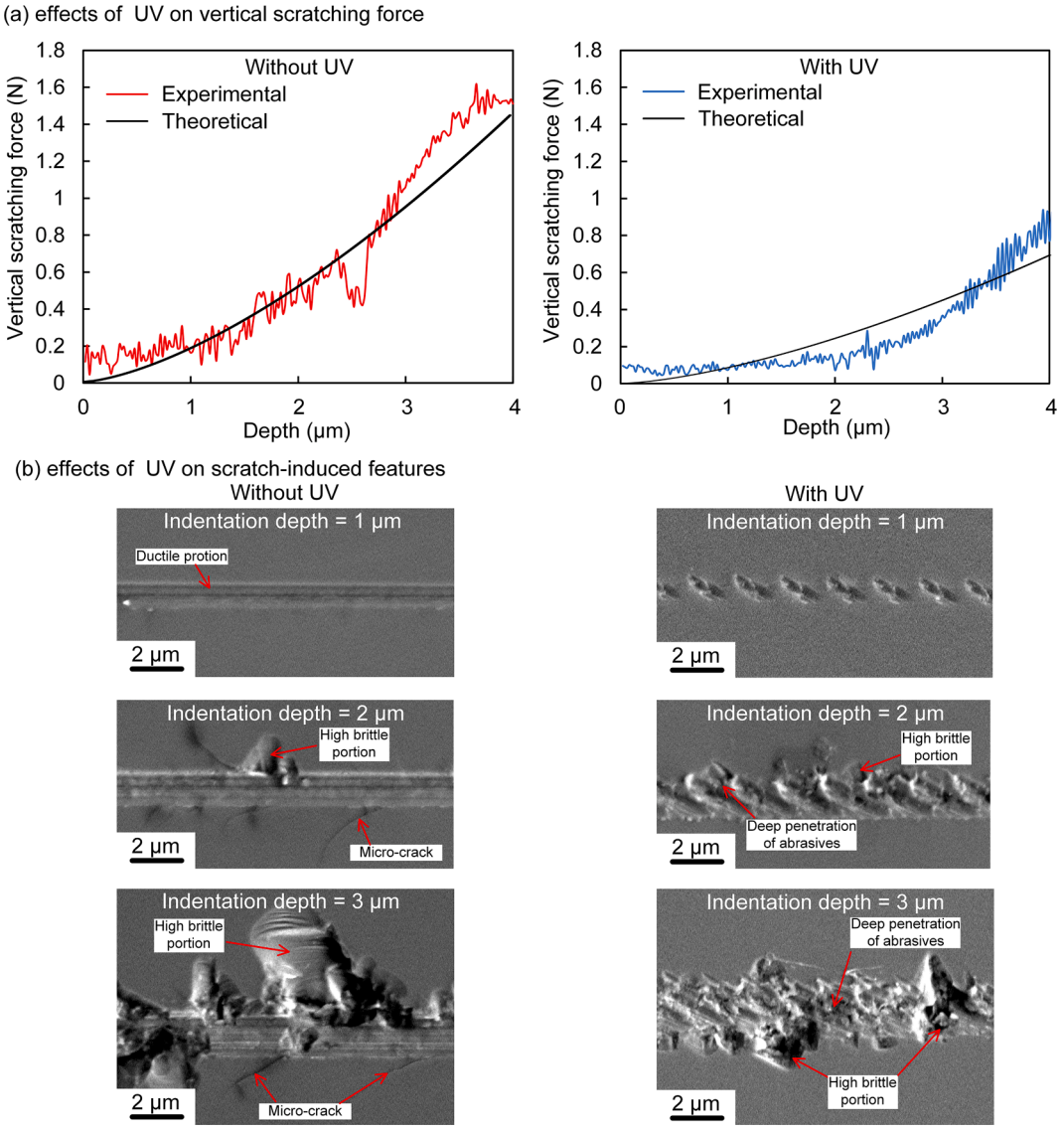

Fig. 5. Effects of ultrasonic vibration on (a) vertical scratching force and (b) scratch-induced features.

material removal to brittle removal. It could also be seen that ultrasonic vibration could reduce the area of high brittle portions and suppress the ductile–brittle transition.

By analyzing the vertical scratching force and the scratch-induced features, the effects of ultrasonic vibration and indentation depth were as follows:

(1) The relationship between the indentation depth and the vertical scratching force could be well expressed by Eq. (8) in the model.
(2) Reducing indentation depth could effectively decrease the vertical scratching force (for a single abrasive) and improve the quality of the machined regions.
(3) When the indentation depth was the same, ultrasonic vibration could decrease the vertical scratching force (for a single abrasive), suppress the brittle material removal, and generate uneven scratch-induced surfaces.

4.2. Effects of ultrasonic vibration and tool rotation speed

4.2.1. Effects on material removal rate (MRR)

Fig. 6 shows the 3D images of the surface micro-machined regions under different tool rotation speeds with and without ultrasonic vibration. Compared with the surface micro-machined regions without ultrasonic vibration, the depths of surface micro-machined regions with ultrasonic vibration were significantly increased. In addition, it could be found that the values of the depth increase (~21 μm – 47 μm) were much greater than the amplitude of the ultrasonic vibration (4 μm). As shown in Fig. 7, silicon particles generated from the RUSμM process were dispersed in the pure water coolant, forming a slurry with silicon abrasive particles. The ultrasonic vibration of the cutting tool induced the movement of silicon abrasive particles. The collision of high-speed abrasive particles with the surface of the silicon wafer resulted in additional material removal. This additional material removal was similar to the ultrasonic machining (USM) process [23,39]. In the USM process, the vibrating tool excited the abrasive particles in the slurry. The brittle material removal caused by the collisions of high-speed abrasive particles was the main material removal mechanism [40]. In addition, the ultrasonic vibration-induced cavitation effects of the slurry were the minor material removal mechanism [41]. Under the action of these two material removal mechanisms, the materials were gently and uniformly removed and the high precision tool shapes were left on the workpiece [42,43].

4.2.2. Effects on single abrasive indentation depth and vertical cutting force

Under each level of tool rotation speed, the single abrasive indentation depth could be reduced by ultrasonic vibration. As shown in Fig. 4 (a), it could be seen that with the assistance of ultrasonic vibration, the abrasive grain's average trajectory length under the conditions of different tool rotation speeds was significantly increased. In most previous studies of the traditional rotary ultrasonic surface machining process, the longer abrasive grain's trajectory length caused by ultrasonic vibration could significantly reduce the indentation depth [44]. However, such a conclusion was not suitable for the RUSμM process. The reason was that in the RUM process, the researchers considered that the MRR was kept unchanged under the condition with and without ultrasonic vibration since the depth of cut and tool diameter were much larger than the ultrasonic vibration amplitude [45]. However, the depth of cut and diameter of the cutting tool in the RUSμM process were small. The additional material removal due to ultrasonic vibration was not negligible. It is necessary to consider the increase of MRR caused by ultrasonic vibration to accurately calculate the indentation depth and cutting force under different conditions. Therefore, as shown in Eq. (11) and Eq. (16), the MRR in the surface micro-machining without and with ultrasonic vibration was calculated, respectively. According to the results from Eq. (12) and Eq. (17), under the condition with ultrasonic vibration, although the MRR was increased, the single abrasive grain's indentation depth was still decreased by the significant increase in abrasive grain's trajectory length.

When the tool rotation speed was increased and the other parameters were kept unchanged, only the trajectory length of the tool abrasive grain was increased while the depth of cut and the number of active abrasive grains on the cutting tool side was unchanged. According to Eqs. (12) and (17), when the number of active abrasive grains on the cutting tool side (n_s) and depth of cut (DOC) were kept unchanged, the single indentation depth (δ) was inversely proportional to the trajectory length of the tool abrasive grain (L_{UV} / $L_{W/O\text{-}UV}$). As a result, the increase of tool rotation speed could decrease the single abrasive indentation depth under conditions both with and without ultrasonic vibration.

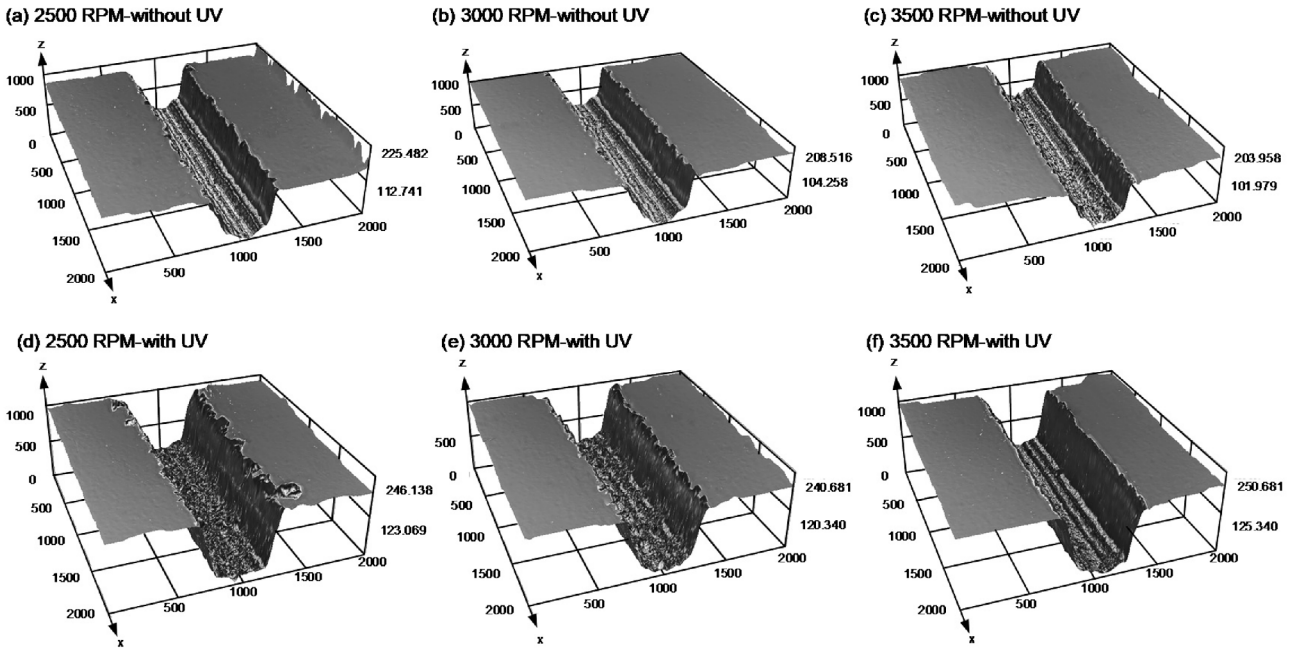

Fig. 6. The 3D images of cutting areas under different tool rotation speeds with and without ultrasonic vibration.

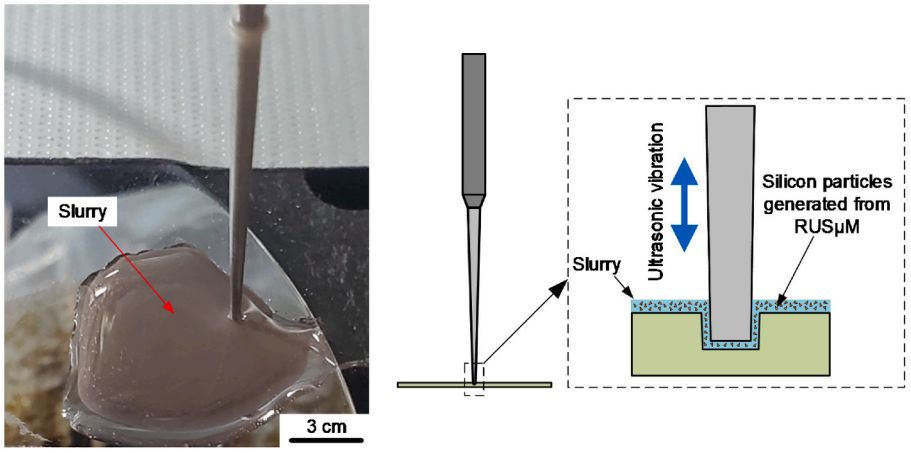

Fig. 7. The illustrations of ultrasonic machining (USM) mechanisms in the rotary ultrasonic surface micro-machining (RUSμM) process.

The experimental and theoretical vertical cutting forces with and without ultrasonic vibration under the conditions of different tool rotation speeds are shown in Fig. 8. Under each level of tool rotation speed, the vertical cutting force was always reduced by ultrasonic vibration. According to Eq. (13), Eq. (18), and the analysis in Section 4.1, the vertical cutting force was positively correlated with the single abrasive indentation depth (δ), the number of active abrasive grains on the cutting tool bottom (n_b), the number of active abrasive grains on the cutting tool bottom (n_s), and the term of ($f{\cdot}\Delta t$) that represented the total indentation time in one ultrasonic cycle. As discussed before, ultrasonic vibration could decrease the single abrasive indentation depth (δ) while the number of active abrasive grains on the cutting tool bottom and side (n_b and n_s) were unchanged. For the term ($f{\cdot}\Delta t$), it has been reported that in the rotary ultrasonic surface machining process, the Δt was smaller than $1/f$ [30]. Therefore, in this study, the term ($f{\cdot}\Delta t$) was less than one. As a result, the decrease of the single abrasive indentation depth (δ) and the accession of the term ($f{\cdot}\Delta t$) less than one led to an effective reduction of the vertical cutting force with the assistance of ultrasonic vibration.

Under both conditions with and without ultrasonic vibration, with the increase of tool rotation speed, the vertical cutting force was decreased. As discussed before, the higher tool rotation speed could result in a smaller single abrasive indentation depth. Meanwhile, the tool rotation speed would not affect the number of active abrasive grains on the cutting tool bottom and side (n_b and n_s) since the depth of cut was unchanged. Similarly, according to Eq. (13), Eq. (18), and the analysis in Section 4.1, the smaller single abrasive indentation depth (δ) could result in the reduction of the vertical cutting force. It also should be noticed that ultrasonic vibration resulted in the significant increase in the standard deviations of the vertical cutting force. The main reason was that the vertical ultrasonic vibration would cause the bottom of the cutting tool to collide with the surface of the silicon wafer, resulting in a greater range of variation in vertical cutting force.

Compared with the experimental and theoretical vertical cutting forces with and without ultrasonic vibration, it could be found that the theoretical vertical cutting force was lower than the experimental vertical cutting force. As discussed in Section 4.1.1, under the condition with ultrasonic vibration, the theoretical depth of surface micro-machining *(DOC + A)* was lower than the experimental depth of surface micro-machining. Therefore, the theoretical MRR with ultrasonic vibration was smaller than the experimental MRR, which led to a lower single abrasive indentation depth and vertical cutting force in the theoretical calculation. In addition, the cutting force generated by USM was not taken into account in the theoretical calculation, which will also lead to the lower theoretical vertical cutting force.

4.2.3. *Effects on the quality of surface micro-machined regions*

Fig. 9 shows the effects of tool rotation speeds on the quality of the surface micro-machined regions with and without ultrasonic vibration. Fig. 9(a) shows the OM images of the contour of the surface micro-machined regions. The experimental results show that when the tool rotation speed was 3000 rpm, ultrasonic vibration could significantly reduce the number and size of additional scratches. With the tool rotation speed further increasing to 3500 rpm, the extremely smooth tool side cutting surface was obtained with the assistance of ultrasonic vibration, whose quality was much higher than that without ultrasonic vibration. As discussed in Section 4.2.2, the assistance of ultrasonic vibration could significantly decrease the single abrasive indentation depth. Based on the findings in Section 4.1, under the condition of relatively small single abrasive indentation depth and with ultrasonic vibration, the material removal mode tended to be dominated by plastic material removal, which had an important impact on the suppression of edge chipping [28,46,47]. However, when the tool rotation speed was

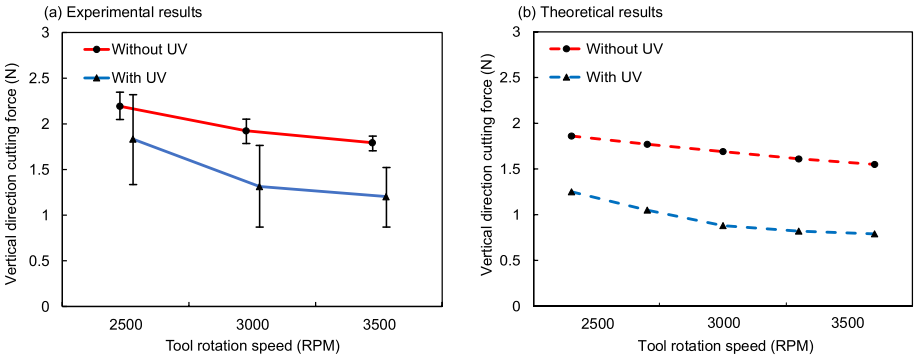

Fig. 8. Effects of the tool rotation speed and ultrasonic vibration on the vertical direction cutting force: (a) experimental results and (b) theoretical results.

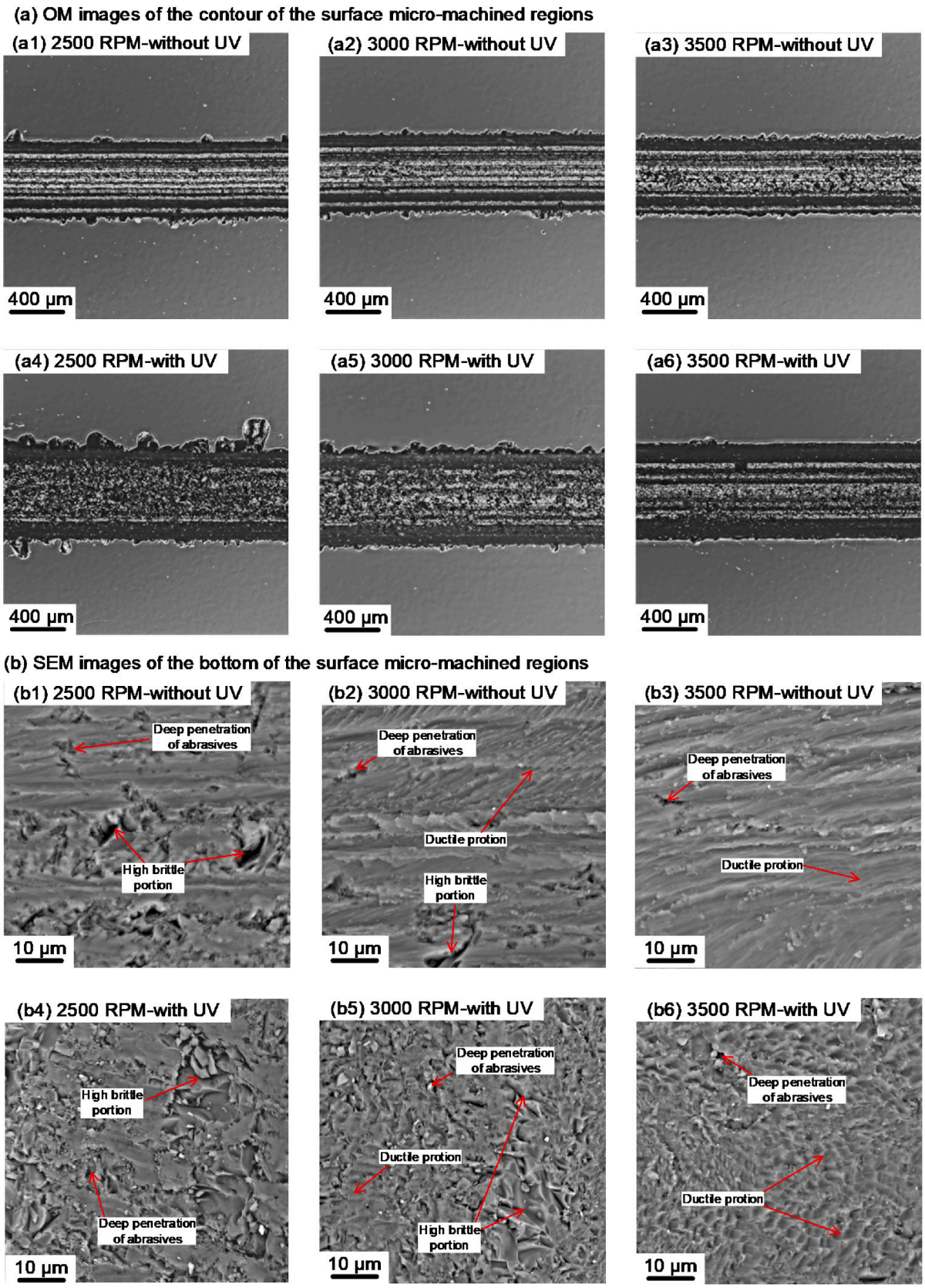

Fig. 9. Effects of tool rotation speeds on the morphology of the surface micro-machined regions with and without ultrasonic vibration: (a) the OM images of the contour of the surface micro-machined regions and (b) the SEM images of the bottom of the surface micro-machined regions.

low (2500 rpm), the ultrasonic vibration had negative effects on the tool side cutting surface quality. Under the condition of 2500 rpm tool rotation speed, the assistance of ultrasonic vibration would generate additional scratches and material removal at the tool side cutting surface. The quality of the tool side cutting surface was even lower than that without ultrasonic vibration. As discussed in Section 4.1.2, under the condition of 2500 rpm tool rotation speed, the existence of ultrasonic vibration could increase the maximum instantaneous vertical cutting force. Due to the extremely small diameter of the cutting tools, the high maximum instantaneous cutting force could lead to the deformation of the cutting tools, which would result in excess material removal and generation of edge chipping. With the increase of the tool rotation speed, the vertical cutting force decreased significantly, thus suppressing this phenomenon.

Fig. 9(b) shows the SEM images of the bottom of the surface micro-machined regions. It could be seen that under each level of tool rotation speed, the bottom of the surface micro-machined regions without ultrasonic vibration showed relatively flat surfaces with some grooves. As a comparison, the bottom of the surface micro-machined regions with ultrasonic vibration showed uneven surfaces with wave shapes. These morphologies were similar to those in the single diamond scratching tests, which were shown in Fig. 5. As discussed in Section 4.1, the reason for these different morphologies was that the contact modes between the abrasives and the substrate were different. Under the conditions without ultrasonic vibration, the continuous contact led to the formation of grooves and relatively flat surfaces. Under the conditions with ultrasonic vibration, the discontinuous contact led to the formation of uneven surfaces. In addition, ultrasonic vibration could reduce the area of high brittle portions. The first reason was that as discussed in Section 4.2.2, ultrasonic vibration could reduce the indentation depth. Based on the analysis in Section 4.1, the smaller indentation depth could suppress microcracks and high brittle portions. The second reason was that the intermittent contact mode induced by ultrasonic vibration also could suppress the microcracks and high brittle portions [27,28], which also was analyzed in Section 4.1.

Under both conditions with and without ultrasonic vibration, with the increase of tool rotation speed, the quality of the surface micro-machined regions was improved. As discussed in Section 4.2.2, the higher tool rotation speed could reduce the indentation depth. Similarly, based on the analysis in Section 4.1, the smaller indentation depth led to the higher quality of the surface micro-machined regions and a less brittle material removal [28,48].

4.2.4. *Effects on the residual stress*

Raman spectrum was based on the interaction of light and materials. Raman spectra usually consisted of a certain number of Raman peaks, each of which represented the wavelength position and intensity of the corresponding Raman scattered light. It has been reported that the Raman peak frequency of stress-free silicon was around 520 cm^{-1} [49]. When residual tensile stress or residual compressive stress was present in the silicon wafers, the bond lengths of the silicon atoms would elongate or shorten accordingly, causing the vibration frequency of the silicon atoms to decrease or increase [50]. The Raman peak would shift to left or right, respectively. At this time, the shift of the Raman peak frequency has a linear relationship with the magnitude of the residual stress inside the silicon wafer [51,52].

Fig. 10 (a) shows the typical Raman spectrum (3000 rpm and 0.2 mm depth of cut) collected from the regions away from the machined surface, the regions of surface micro-machined regions without ultrasonic vibration, and the regions of surface micro-machined region with ultrasonic vibration. The Raman peak position of the regions away from the machined surface was 520.2 cm^{-1}, which was the same as the reported Raman peak position in other investigations [49]. After the surface micro-machining without ultrasonic vibration, the Raman peak position shifted to the right to 527.2 cm^{-1}. As discussed before, such a phenomenon indicated the presence of residual compressive stress. As a comparison, with the assistance of ultrasonic vibration, the Raman peak position shifted less to the right, reaching around 523.3 cm^{-1}. The less rightward shift of the Raman peak position indicated that ultrasonic vibration was effective in reducing the residual compressive stress. The major reason was that ultrasonic vibration could reduce both single abrasive vertical scratching force and vertical direction cutting force, which was discussed in Section 4.1 and Section 4.2.3, respectively. Thus, the damage to the crystal structure of silicon wafers in the machining process was reduced, resulting in lower residual compressive stress. Similar results were also reported in the surface machining process of other brittle materials such as sapphire wafers [53].

Fig. 10(b) shows the effects of tool rotation speed and ultrasonic vibration on the measured Raman peak positions. Under both conditions with and without ultrasonic vibration, with the increase of tool rotation speed, the rightward shift of Raman peak positions became less, indicating the lower residual compressive stress. Similarly, this phenomenon can be attributed to the fact that a higher tool rotation speed reduced the single abrasive indentation depth, thus reducing the single abrasive vertical scratching force and the vertical direction cutting force

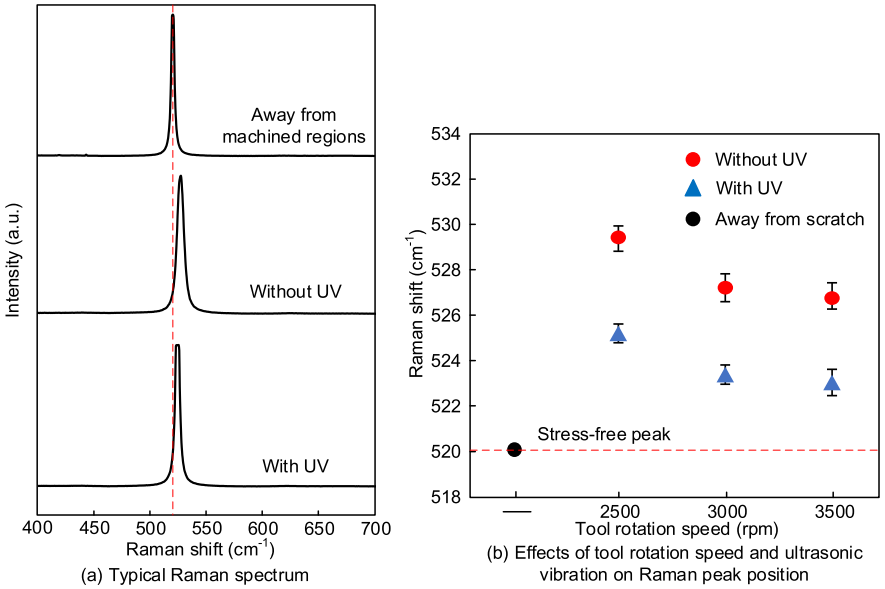

Fig. 10. The typical Raman spectrum and the effects of tool rotation speed and ultrasonic vibration on Raman peak position.

[53,54].

4.3. Effects of the depth of cut

4.3.1. Effects on material removal rate (MRR)

Fig. 11 shows the 3D images of cutting areas under the conditions of different depths of cut with and without ultrasonic vibration. It could be seen that the ultrasonic vibration could effectively increase the depth of surface micro-machining. In addition, with the increase of the depth of cut from 0.1 mm to 0.3 mm, the values of the depth increase caused by ultrasonic vibration increased from 22 μm to 58 μm. This indicated that as the depth of cut increased, ultrasonic vibration had a greater effect on increasing MRR. The reason was that with the increase of depth of cut, more material was removed from the surface of the silicon wafer. There were more abrasive silicon particles generated during the surface micro-machining process. The higher concentration of abrasive particles in the slurry could promote the additional USM material removal [55].

4.3.2. Effects on single abrasive indentation depth and vertical cutting force

As discussed in Section 4.2.2, the single abrasive indentation depth was related to the depth of cut (*DOC*), the active abrasive grains on the cutting tool side (n_s), and the trajectory lengths of the tool abrasive grain (L_{UV} / $L_{W/O\text{-}UV}$). The relationship between the active abrasive grains on the cutting tool side (n_s) and depth of cut (*DOC*) could be achieved by Eq. (19) [45,56]:

$$n_s = \pi \cdot DOC(DOC tan(3.2^{\circ}) + R_B) \cdot C_a \tag{19}$$

Where *Ca* is the abrasive concentration of the cutting tool, Num/mm.

Substituting Eq. (19) into Eq. (12) and Eq. (17) respectively, it could be found that the term of $DOC(DOC tan(3.2^{\circ}) + R_B)$ was removed from the left side and right side of Eq. (12) and Eq. (17). In addition, according to Eq. (4) and Eq. (7), when the depth of cut (*DOC*) was increased and the other parameters were unchanged, the trajectory lengths of tool abrasive grain under the conditions with and without ultrasonic vibration (L_{UV} / $L_{W/O\text{-}UV}$) were kept unchanged. Due to these reasons, when using the same tool (the same abrasive concentration of the cutting tool), the increase of depth of cut would not affect the single abrasive indentation depth.

Fig. 12 shows the effects of depth of cut and ultrasonic vibration on the vertical direction cutting force. Under all different depths of cut levels, the assistance of ultrasonic vibration could reduce the vertical cutting force. The reasons for this result were explained in detail in Section 4.2.2. With the increase of depth of cut, the vertical direction cutting forces under both conditions without and with ultrasonic vibration were increased. When the depth of cut increased, the active abrasive grains on the cutting tool side (n_s) would be significantly increased as shown in Eq. (19). The number of active abrasive grains on the cutting tool bottom (n_b) was unchanged since the cutting tools used in each group of experiments were the same. The single abrasive indentation depth (δ) was also kept unchanged as discussed before. According to Eq. (13) and Eq. (18), as the depth of cut increased, the large active abrasive grains on the cutting tool side (n_s) resulted in the larger vertical direction cutting force.

The experimental results also showed that the larger cutting depth could enhance the reducing effects of ultrasonic vibration on vertical cutting force. However, the theoretical results did not reflect this phenomenon. The main reason was that the cutting forces caused by the USM material removal mechanism were not considered in the theoretical calculations. When the depth of cut was large, there were much more silicon particles generated during the surface micro-machining process. The role of USM material removal mechanisms with lower cutting force had a greater impact on the reduction of vertical cutting force. In addition, the indentation depth in the vertical direction was difficult to be obtained directly. In this study, the indentation depth in the vertical direction was obtained by approximating it to be equal to the indentation depth in the horizontal direction [57]. Although this model could effectively analyze the effects of parameters and ultrasonic vibrations on the vertical cutting forces, it was still difficult to accurately obtain the actual vertical cutting forces measured in the experiments.

4.3.3. Effects on the quality of surface micro-machined regions

Fig. 13 shows the cutting surface under the conditions of different depths of cut with and without ultrasonic vibration. Fig. 13(a) shows the OM images of the contour of the surface micro-machined regions. Under each level of depth of cut, the number and size of additional scratches

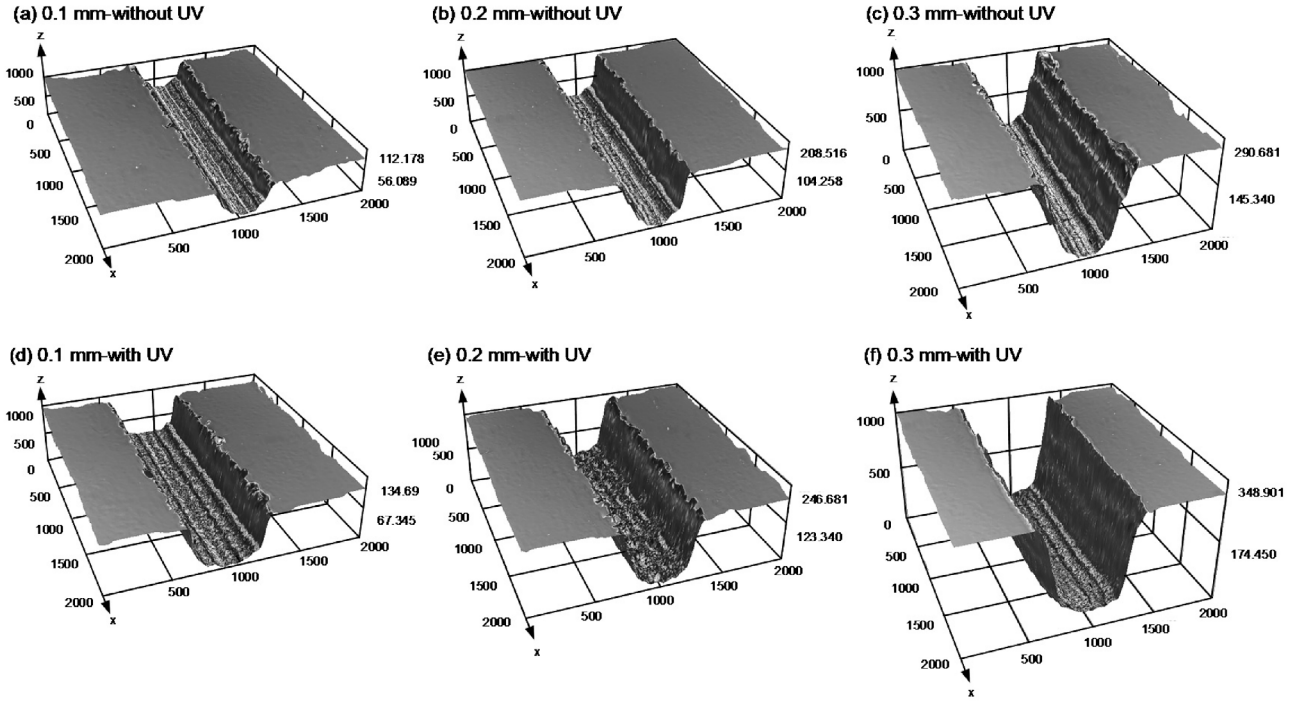

Fig. 11. The 3D images of cutting areas under different depths of cut with and without ultrasonic vibration.

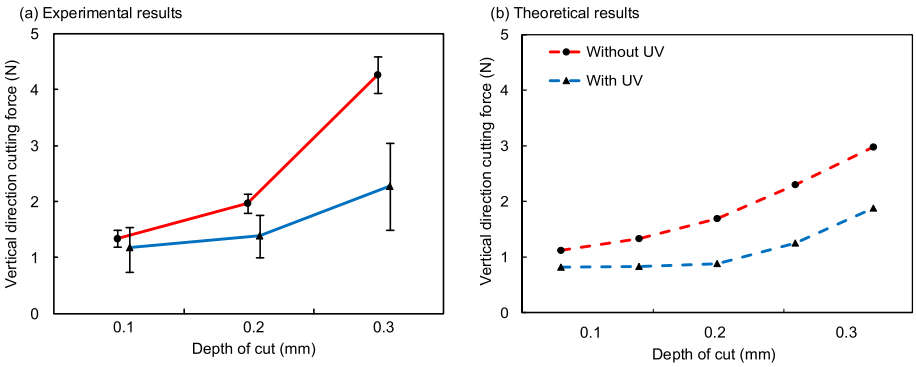

Fig. 12. Effects of the depth of cut and ultrasonic vibration on the vertical direction cutting force: (a) experimental results and (b) theoretical results.

and edge chipping were reduced with the assistance of ultrasonic vibration. The reasons for ultrasonic vibration to reduce edge chipping had been discussed in detail in Section 4.2.3. In addition, when the depth of cut was at a high level, ultrasonic vibration could greatly increase the quality of the tool side cutting surface. The major reason was that under the conditions of large depth of cut, ultrasonic vibration was more effective in reducing vertical cutting forces, which could better reduce the deformation of the cutting tools and thus further reduce the excess irregular material removal [58].

Fig. 13(b) shows the SEM images of the bottom of the surface micro-machined regions. It could be seen that ultrasonic vibration resulted in uneven surfaces and reduced the area of high brittle portions under each level of depth of cut, which was similar to the results in Section 4.2.3. Different from the effects of tool rotation speed, the depth of cut had almost no effect on the quality of the bottom of the surface micro-machined regions. As discussed in Section 4.3.2, the single abrasive indentation depth was kept unchanged as the increase of depth of cut. In addition, the cutting force directly on the bottom of the surface micro-machined regions was kept constant. The increase in the vertical cutting force was mainly due to the increase in the vertical downward component force on the side of the cutting tool (caused by the increase in the number of abrasives on the tool side). Based on the analysis in Section 4.1, the similar indentation depth and vertical cutting force led to the similar material removal mechanisms and virtually unchanged quality of the bottom of the surface micro-machined regions [27,59].

4.3.4. *Effects on the residual stress*

Fig. 14 shows the measured Raman peak positions under different levels of depth cut with and without ultrasonic vibration. Under each level of depth of cut, the rightward shift of Raman peak position was reduced with the assistance of ultrasonic vibration. These results proved once again that ultrasonic vibration was effective in reducing residual compressive stresses caused by the surface micro-machining process. Under both conditions with and without ultrasonic vibration, with the increase of depth of cut, there was almost no change in the shift of Raman peak positions. Although increasing the depth of cut resulted in a higher vertical cutting force, it would not increase the residual compressive stress on the bottom surface. The first reason was that as discussed in Section 4.3.2, the larger depth of cut would not increase the single abrasive indentation depth. According to the analysis in Section 4.1, under the same single abrasive indentation depth, the single abrasive vertical scratching force would not significantly change, resulting in similar residual compressive stress. Secondly, as discussed in Section 4.3.3, the additional vertical cutting forces caused by the larger depth of cut were concentrated on the cutting tool side rather than on the cutting tool bottom. Therefore, the residual compressive stress at the bottom of the surface micro-machining regions would not significantly change [53,54].

5. Conclusion

In this study, the brittle material (silicon wafer) was surface machined by the RUSμM process. The tool abrasive grain's trajectory and vertical cutting force in the RUSμM process and traditional surface micro-machining process were analyzed by combining the experimental results and theoretical calculations, respectively. The effects of ultrasonic vibration on the MRR, vertical cutting force, cutting surface quality, and residual stress under different conditions of tool rotation speed and depth of cut were experimentally and theoretically investigated for the first time. The following conclusions had been achieved.

1. Ultrasonic vibration could increase the MRR since the ultrasonic vibration increased the depth of cut. In addition, materials were also removed due to a similar material removal mechanism to USM.
2. Under most combinations of the input parameter, ultrasonic vibration could reduce the vertical cutting force, suppress the generation of high brittle portions in the bottom of the surface micro-machined regions, and reduce the residual compressive stress by decreasing the single abrasive indentation depth and providing intermittent contact mode between cutting tool and silicon wafer. However, ultrasonic vibration could cause the uneven cutting surface on the bottom regions due to the intermittent contact mode.
3. Under the conditions of low tool rotation speeds, ultrasonic vibration had negative impacts on the cutting surface quality since the higher maximum instantaneous cutting forces resulted in the deformation of the tool.
4. The higher tool rotation speed could improve the quality of the bottom of the surface micro-machined regions and reduce the residual compressive stress since the increase in trajectory length of abrasive grains could effectively reduce the single abrasive indentation depth.
5. The increase in the depth of cut could increase the vertical cutting force. However, the depth of cut has almost no effect on the quality of the bottom of the surface micro-machined regions and the residual compressive stress. Theoretical calculations and experimental results confirmed that the increased vertical cutting force with the depth of cut was caused by more abrasives on the cutting tool side, and the single abrasive indentation depth at the bottom surface did not change.

CRediT authorship contribution statement

Yunze Li: Conceptualization, Methodology, Investigation, Data curation, Writing – original draft, Writing – review & editing. **Dongzhe Zhang:** Investigation, Data curation, Writing – original draft, Writing – review & editing. **Hui Wang:** Investigation, Writing – review & editing. **Gaihua Ye:** Data curation. **Rui He:** Data curation. **Weilong Cong:** Conceptualization, Methodology, Investigation, Data curation, Writing – original draft, Writing – review & editing, Funding acquisition.

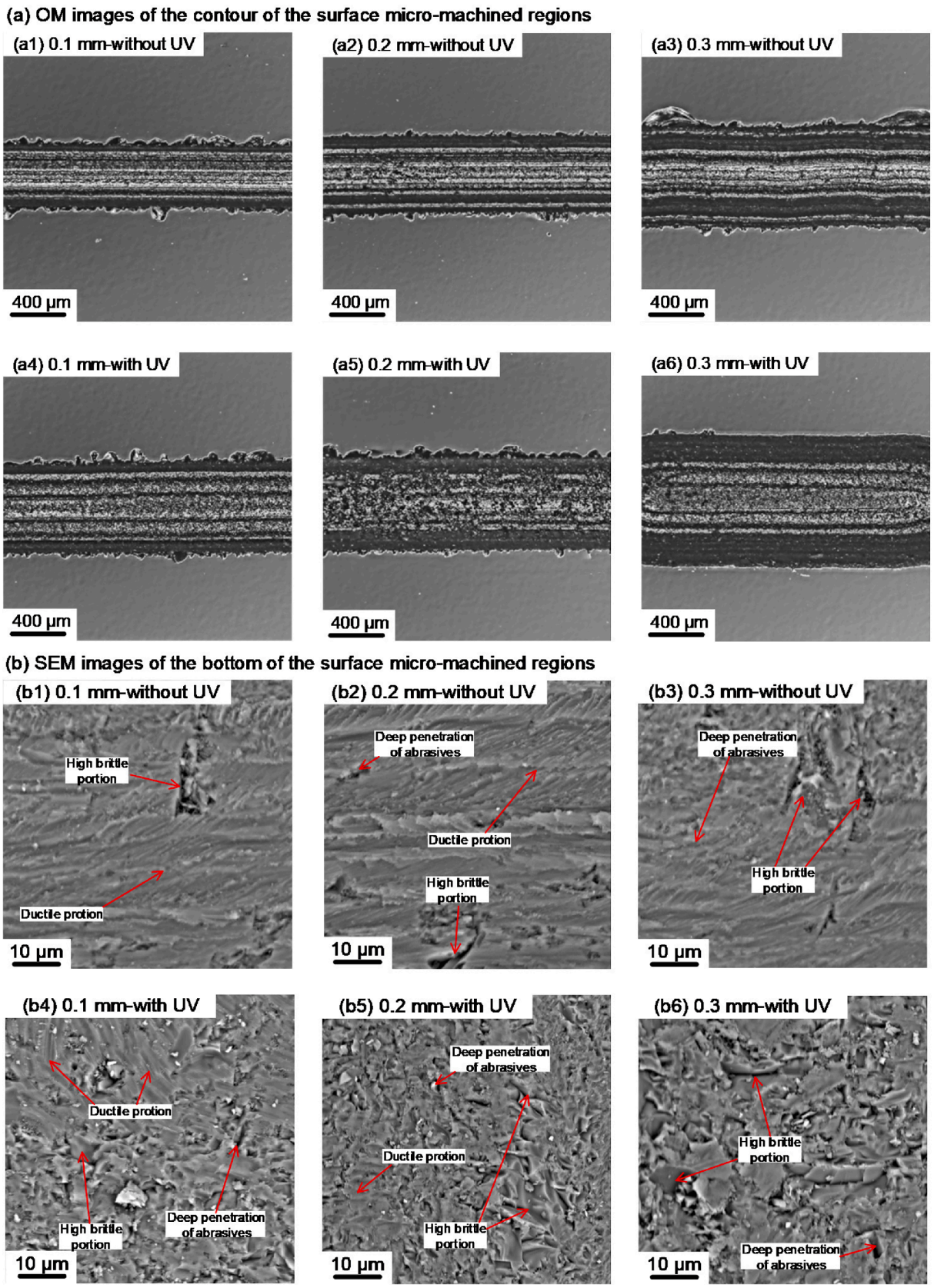

Fig. 13. Effects of the depth of cut on cutting surface morphology with and without ultrasonic vibration: (a) the OM images of the contour of the surface micro-machined regions and (b) the SEM images of the bottom of the surface micro-machined regions.

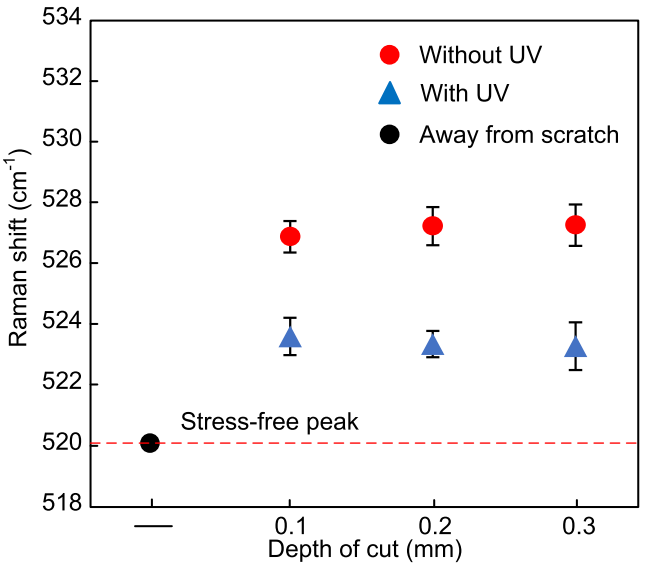

Fig. 14. The effects of depth of cut and ultrasonic vibration on Raman peak position.

Declaration of Competing Interest

The authors declare that they have no known competing financial interests or personal relationships that could have appeared to influence the work reported in this paper.

Data availability

Data will be made available on request.

Acknowledgment

The work was supported by U.S. National Science Foundation through the award CMMI- 2102181.

References

[1] D. Dornfeld, S. Min, Y. Takeuchi, Recent advances in mechanical micromachining, CIRP Ann. 55 (2) (2006) 745–768.
[2] M. Elwenspoek, H.V. Jansen, Silicon micromachining, vol. 7, Cambridge University Press, 2004.
[3] R.T. Howe, Surface micromachining for microsensors and microactuators, J. Vacuum Sci. Technol. B 6 (6) (1988) 1809–1813.
[4] W. Kern, The evolution of silicon wafer cleaning technology, J. Electrochem. Soc. 137 (6) (1990) 1887–1892.
[5] D.-H. Neuhaus, A. Münzer, Industrial silicon wafer solar cells, Adv. OptoElectron. 2007 (2007) 1–15.
[6] M.H. Cohen, K. Melnik, A.A. Boiarski, M. Ferrari, F.J. Martin, Microfabrication of silicon-based nanoporous particulates for medical applications, Biomed. Microdevices 5 (3) (2003) 253–259.
[7] Q.-Y. Tong, U. Gösele, Semiconductor wafer bonding: recent developments, Mater. Chem. Phys. 37 (2) (1994) 101–127.
[8] L. Giulio, B. Marco, F. Aldo, T.P. Domenico, M. Mario, Microthrusters in silicon for aerospace application, IEEE Aerospace Electron. Syst. Mag. 17 (9) (2002) 22–27.
[9] N. Kannan, D. Vakeesan, Solar energy for future world:-A review, Renew. Sustain. Energy Rev. 62 (2016) 1092–1105.
[10] E.K. Antwi, K. Liu, H. Wang, A review on ductile mode cutting of brittle materials, Front. Mech. Eng. 13 (2) (2018) 251–263.
[11] P. Pal, K. Sato, A comprehensive review on convex and concave corners in silicon bulk micromachining based on anisotropic wet chemical etching, Micro Nano Syst. Lett. 3 (1) (2015) 1–42.
[12] D. Reynaerts, W. Meeusen, H. Van Brussel, Machining of three-dimensional microstructures in silicon by electro-discharge machining, Sensors Actuators A: Physical 67 (1–3) (1998) 159–165.
[13] M. Singh, S. Singh, S. Kumar, Experimental investigation for generation of micro-holes on silicon wafer using electrochemical discharge machining process, Silicon 12 (7) (2020) 1683–1689.
[14] H.-J. Wang, T. Yang, A review on laser drilling and cutting of silicon, J. Eur. Ceram. Soc. 41 (10) (2021) 4997–5015.
[15] R. Melentiev, F. Fang, Recent advances and challenges of abrasive jet machining, CIRP J. Manuf. Sci. Technol. 22 (2018) 1–20.
[16] D.-S. Park, M.-W. Cho, H. Lee, W.-S. Cho, Micro-grooving of glass using micro-abrasive jet machining, J. Mater. Process. Technol. 146 (2) (2004) 234–240.
[17] N. Haghbin, J.K. Spelt, M. Papini, Abrasive waterjet micro-machining of channels in metals: comparison between machining in air and submerged in water, Int. J. Mach. Tools Manuf. 88 (2015) 108–117.
[18] M.S. Amer, M. El-Ashry, L.R. Dosser, K. Hix, J.F. Maguire, B. Irwin, Femtosecond versus nanosecond laser machining: comparison of induced stresses and structural changes in silicon wafers, Appl. Surf. Sci. 242 (1–2) (2005) 162–167.
[19] M. Itano, F.W. Kern, M. Miyashita, T. Ohmi, Particle removal from silicon wafer surface in wet cleaning process, IEEE Trans. Semicond. Manuf. 6 (3) (1993) 258–267.
[20] T. Corman, P. Enoksson, G. Stemme, Deep wet etching of borosilicate glass using an anodically bonded silicon substrate as mask, J. Micromech. Microeng. 8 (2) (1998) 84–87.
[21] Z. Yang, L. Zhu, G. Zhang, C. Ni, B. Lin, Review of ultrasonic vibration-assisted machining in advanced materials, Int. J. Mach. Tools Manuf. 156 (2020) 103594.
[22] R.P. Singh, S. Singhal, Rotary ultrasonic machining: a review, Mater. Manuf. Process. 31 (14) (2016) 1795–1824.
[23] G. Ya, H. Qin, S. Yang, Y. Xu, Analysis of the rotary ultrasonic machining mechanism, J. Mater. Process. Technol. 129 (1–3) (2002) 182–185.
[24] K. Yamada, M. Yamada, H. Maki, K. Itoh, Fabrication of arrays of tapered silicon micro-/nano-pillars by metal-assisted chemical etching and anisotropic wet etching, Nanotechnology 29 (28) (2018) 28LT01.
[25] A. Luft, U. Franz, L. Emsermann, J. Kaspar, A study of thermal and mechanical effects on materials induced by pulsed laser drilling, Appl. Phys. A 63 (2) (1996) 93–101.
[26] L. O'Toole, C. Kang, F. Fang, Advances in rotary ultrasonic-assisted machining, Nanomanuf. Metrol. 3 (1) (2020) 1–25.
[27] R.P. Singh, S. Singhal, Experimental investigation of machining characteristics in rotary ultrasonic machining of quartz ceramic, Proceed. Inst. Mech. Eng., Part L 232 (10) (2018) 870–889.
[28] R.P. Singh, S. Singhal, An experimental study on rotary ultrasonic machining of macor ceramic, Proceed. Inst. Mech. Eng., Part B 232 (7) (2018) 1221–1234.
[29] D.R. Unune, H.S. Mali, Current status and applications of hybrid micro-machining processes: a review, Proceed. Inst. Mech. Eng., Part B 229 (10) (2015) 1681–1693.
[30] S. Das, B. Doloi, B. Bhattacharyya, Recent Advancement on Ultrasonic Micro Machining (USMM) Process, in: Non-traditional Micromachining Processes, Springer, 2017, pp. 61–91.
[31] Sarwade, A., Sundaram, M., Rajurkar, K. (2010). Investigation of micro hole drilling in bovine rib using micro rotary ultrasonic machining. In *16th International Symposium on Electromachining, ISEM 2010*.
[32] F. Ning, Y. Hu, Z. Liu, W. Cong, Y. Li, X. Wang, Ultrasonic vibration-assisted laser engineered net shaping of Inconel 718 parts: a feasibility study, Procedia Manuf. 10 (2017) 771–778.
[33] H. Wang, Z.J. Pei, W. Cong, A feeding-directional cutting force model for end surface grinding of CFRP composites using rotary ultrasonic machining with elliptical ultrasonic vibration, Int. J. Mach. Tools Manuf. 152 (2020) 103540.
[34] J. Wang, J. Zhang, P. Feng, P. Guo, Damage formation and suppression in rotary ultrasonic machining of hard and brittle materials: a critical review, Ceram. Int. 44 (2) (2018) 1227–1239.
[35] F. Ning, W. Cong, H. Wang, Y. Hu, Z. Hu, Z. Pei, Surface grinding of CFRP composites with rotary ultrasonic machining: a mechanistic model on cutting force in the feed direction, Int. J. Adv. Manuf. Technol. 92 (1) (2017) 1217–1229.
[36] J. Cao, Y. Wu, D. Lu, M. Fujimoto, M. Nomura, Material removal behavior in ultrasonic-assisted scratching of SiC ceramics with a single diamond tool, Int. J. Mach. Tools Manuf. 79 (2014) 49–61.
[37] Z. Liang, X. Wang, Y. Wu, L. Xie, L. Jiao, W. Zhao, Experimental study on brittle–ductile transition in elliptical ultrasonic assisted grinding (EUAG) of monocrystal sapphire using single diamond abrasive grain, Int. J. Mach. Tools Manuf. 71 (2013) 41–51.
[38] T.T. Öpöz, X. Chen, Experimental investigation of material removal mechanism in single grit grinding, Int. J. Mach. Tools Manuf. 63 (2012) 32–40.
[39] K. Seah, Y. Wong, L. Lee, Design of tool holders for ultrasonic machining using FEM, J. Mater. Process. Technol. 37 (1–4) (1993) 801–816.
[40] G. Kainth, A. Nandy, K. Singh, On the mechanics of material removal in ultrasonic machining, Int. J. Mach. Tool Des. Res. 19 (1) (1979) 33–41.
[41] V. Soundararajan, V. Radhakrishnan, An experimental investigation on the basic mechanisms involved in ultrasonic machining, Int. J. Mach. Tool Des. Res. 26 (3) (1986) 307–321.
[42] P. Guzzo, A. Shinohara, A. Raslan, A comparative study on ultrasonic machining of hard and brittle materials, J. Braz. Soc. Mech. Sci. Eng. 26 (2004) 56–61.
[43] J. Wang, J. Zhang, P. Feng, P. Guo, Q. Zhang, Feasibility study of longitudinal–torsional-coupled rotary ultrasonic machining of brittle material, J. Manuf. Sci. Eng. 140 (5) (2018).
[44] W. Cong, F. Ning, A fundamental investigation on ultrasonic vibration-assisted laser engineered net shaping of stainless steel, Int. J. Mach. Tools Manuf. 121 (2017) 61–69.
[45] H. Wang, D. Zhang, Y. Li, W. Cong, The effects of elliptical ultrasonic vibration in surface machining of CFRP composites using rotary ultrasonic machining, The International Journal of Advanced Manufacturing Technology 106 (11) (2020) 5527–5538.
[46] R.P. Singh, S. Singhal, Experimental study on rotary ultrasonic machining of alumina ceramic: Microstructure analysis and multi-response optimization,

Proceedings of the Institution of Mechanical Engineers, Part L: Journal of Materials: Design and Applications 232 (12) (2018) 967–986.
[47] R.P. Singh, R. Kataria, S. Singhal, R. Garg, M. Tyagi, Hole quality measures in rotary ultrasonic drilling of silicon dioxide (SiO2): investigation and modeling through designed experiments, Silicon 12 (11) (2020) 2587–2600.
[48] R.P. Singh, S. Singhal, Investigation of machining characteristics in rotary ultrasonic machining of alumina ceramic, Materials manufacturing processes 32 (3) (2017) 309–326.
[49] R. Tsu, J.G. Hernandez, Temperature dependence of silicon Raman lines, Appl. Phys. Lett. 41 (11) (1982) 1016–1018.
[50] Ge, J., Stangl, R., AG, A., & Mueller, T. (2013). Detailed micro Raman spectroscopy analysis of doped silicon thin film layers and its feasibility for heterojunction silicon wafer solar cells. *Journal of Materials Science Chemical Engineering, 2013*.
[51] Y. Gogotsi, C. Baek, F. Kirscht, Raman microspectroscopy study of processing-induced phase transformations and residual stress in silicon, Semiconductor Science Technology 14 (10) (1999) 936–944.
[52] L. Zhen-Kun, K. Yi-Lan, H. Ming, Q. Yu, X. Han, N. Hong-Pan, An experimental analysis of residual stress measurements in porous silicon using micro-Raman spectroscopy, Chin. Phys. Lett. 21 (2) (2004) 403–405.
[53] C. Zhang, P. Feng, J. Zhang, Ultrasonic vibration-assisted scratch-induced characteristics of C-plane sapphire with a spherical indenter, Int. J. Mach. Tools Manuf. 64 (2013) 38–48.
[54] Y. Gogotsi, G. Zhou, S.-S. Ku, S. Cetinkunt, Raman microspectroscopy analysis of pressure-induced metallization in scratching of silicon, Semicond. Sci. Technol. 16 (5) (2001) 345–352.
[55] M. Komaraiah, P. Narasimha Reddy, Rotary ultrasonic machining—a new cutting process and its performance, Int. J. Prod. Res. 29 (11) (1991) 2177–2187.
[56] F. Ning, H. Wang, W. Cong, P. Fernando, A mechanistic ultrasonic vibration amplitude model during rotary ultrasonic machining of CFRP composites, Ultrasonics 76 (2017) 44–51.
[57] F. Ning, H. Wang, Y. Hu, W. Cong, M. Zhang, Y. Li, Rotary ultrasonic surface machining of CFRP composites: a comparison with conventional surface grinding, Procedia Manuf. 10 (2017) 557–567.
[58] K.S. Woon, M. Rahman, The effect of tool edge radius on the chip formation behavior of tool-based micromachining, Int. J. Adv. Manuf. Technol. 50 (9) (2010) 961–977.
[59] R.P. Singh, S. Singhal, Rotary ultrasonic machining of macor ceramic: an experimental investigation and microstructure analysis, Mater. Manuf. Process. 32 (9) (2017) 927–939.